Available online at www.sciencedirect.com
ScienceDirect
International Journal of Heat and Mass Transfer 50 (2007) 640–653
International Journal of HEAT and MASS TRANSFER
www.elsevier.com/locate/ijhmt

Heat transfer characteristics of three interacting methane/air flame jets impinging on a flat surface

Subhash Chander, Anjan Ray *

Department of Mechanical Engineering, Indian Institute of Technology, Delhi, New Delhi 110 016, India

Received 22 September 2005; received in revised form 30 June 2006
Available online 22 September 2006

Abstract

An experimental study has been conducted for three interacting methane/air flame jets (arranged in a triangular configuration) impinging normally on a flat surface. Surface heat flux distributions have been determined for various dimensionless inter-jet spacings ($S/d = 3$, 4, 6 and 7.58) and separation distances between the exit plane of the burners and the target plate ($H/d = 2$, 2.6, 5 and 7). All experiments were conducted for stoichiometric mixture at a Reynolds number of 800. The surface heat flux distributions were intimately related to flame shapes. For small inter-jet spacings and small separation distances, flames were deflected outward from the centroid of the triangular arrangement due to strong interaction between the jets. The heating was quite non-uniform at very large inter-jet spacings. Zones of low heat flux were obtained when the tip of inner reaction zones were intercepted by the plate ($H/d = 2$). There were sharp peaks in the heat flux distribution when the tips of the inner reaction zones just touched the impingement surface ($H/d = 2.6$). Heat flux distribution was non-uniform at small separation distances ($H/d = 2$ and 2.6). For the system of flame jets under consideration, the optimum configuration, considering the magnitude of the average heat flux and the uniformity in the heat flux distribution, was corresponding to $H/d = 5$ and $S/d = 3$.

Keywords: Interacting flame jets; Impingement; Heat transfer; Premixed flame; Flat surface

1. Introduction

Rapid and uniform heating of materials is necessary to ensure material quality in glass and metal processing industries. Flame impingement heating is one of the efficient ways of heating a surface. Not only high heat transfer coefficients are obtained, but by using a number of jets, the surface heat transfer distribution can also be controlled. However, achieving optimum heat transfer during flame impingement heating for a specific purpose is still a challenge. This is because of the large number of parameters involved, e.g., burner shape, array configuration, distance of the burners from the impingement surface, inter-jet spacing, geometry and inclination of the impingement surface, initial flow field and turbulence intensity in the jet, the surrounding near field boundary conditions and so on.

Literature on heat transfer from arrays of jets is primarily on isothermal jets. Saripalli [1] conducted flow visualization of a multiple-jet impingement. A fountain between two adjacent jets was observed. The interaction between the fountain and the two jets was found to increase with decrease in the jet spacing. San and Lai [2] investigated the effect of jet interference before impingement and jet fountain on the heat transfer. With increase in jet-to-jet spacing, the fountain effect rapidly diminished, resulting in increase in stagnation point Nusselt number. Behbahani and Goldstein [3] experimentally determined the two-dimensional distribution of local heat transfer from a plate to an array of staggered circular impinging air jets. Goldstein and Seol [4] investigated the recovery factor, effectiveness and heat transfer coefficient distribution for a single row of impinging circular air jets. It was found that for a

* Corresponding author. Tel.: +91 11 26591143; fax: +91 11 26582053.
E-mail address: raya@mech.iitd.ernet.in (A. Ray).

0017-9310/$ - see front matter © 2006 Elsevier Ltd. All rights reserved.
doi:10.1016/j.ijheatmasstransfer.2006.07.011

Nomenclature

A	impingement surface area (mm^2)
A/F	air/fuel ratio
d	burner diameter (mm)
H/d	non-dimensional separation distance between the burner exit plane and the impingement surface
JT	tip of the inner reaction cone just touching the impingement surface
M	molecular weight (kg/kmol)
n	number of measurements
O	centroid
$\dot{q}''$	heat flux
r	radial distance (mm)
r/d	non-dimensional radial distance
Re	Reynolds number
RJRC	radial jet re-attachment combustion
S	inter-jet spacing (mm)
S/d	non-dimensional inter-jet spacing
u	flow velocity (m/s)
X, Y	coordinate axes in the plane of impingement plate
y	mole fraction

Greek symbols

μ	dynamic viscosity (kg/m s)
ρ	density (kg/m^3)
ϕ	equivalence ratio
θ	angular direction on the impingement surface (deg)

Subscripts

actual	actual state
dev	deviation
e	equivalent
exit	at the exit
i	index for species (CH_4 or O_2 or N_2)
mix	air/fuel mixture
rms	root mean square
stoic	stoichiometric mixture

given Reynolds number, the arrays with closer jet-to-jet spacing produced large average Nusselt numbers. A single row of jet appeared to be more efficient than a slot jet for maximizing the heat transfer with the same mass flow rate. Metzger et al. [5] measured the heat transfer characteristics for two-dimensional arrays of jets impinging on a surface parallel to the orifice plate. Small center-to-center distance between the adjacent jets resulted in interference of the effluents from neighboring jets. It was seen that the inline configuration was better than the staggered configuration when cross-flow effects were large. Can et al. [6] measured average heat transfer coefficients under arrays of both slot nozzles and circular holes. Also, the relationships between the heat transfer coefficient, air mass flow rate and fan power were developed. Huber and Viskanta [7] studied the convective heat transfer to confined isothermal impinging gas jet arrays. It was found that for an array at larger separation distance (of the order of six times diameter), adjacent jet interference before impingement causes significant degradation of convective coefficient when compared to single jet. Huber and Viskanta [8] found different shapes of contours for center jets and perimeter jets. Goldstein and Timmers [9] observed that in multiple impinging jets, flow interaction can cause mixing induced turbulence which causes local minimum at the stagnation point to be absent at small separation distances. Geers et al. [10] observed that the center jet in the array of jets has the shortest core and the highest turbulent kinetic energy, indicative of strong interaction with a large number of surrounding jets. Obot and Trabold [11] investigated the effect of spent air exit scheme on heat transfer of impinging jets and found that the minimum cross-flow scheme showed the best performance followed by intermediate and maximum cross-flows. Saad et al. [12] used the concept of flow cell, which is the volume contained by the impingement and the confinement surfaces and the centerlines of the adjacent inlet nozzles and exhaust ports, to analyze the confined multiple impinging slot jet system with symmetric exit port in the confinement surface. Slayzak et al. [13] studied the interaction between circular, free surface jets aligned in a single row, as well as interactions in an inline array of two such rows for free surface liquid jets impinging on constant heat flux surface. Florschuets and Su [14] studied the effect of cross-flow temperature on heat transfer within an array of impinging air jets.

Literature is rather limited for arrays of flame jet impingement. Dong et al. [15–18] studied the heat transfer characteristics of three inline laminar flame jets forming a subset of an inline array of flame jets. They inferred from their experiments that a positive pressure was produced at the jet interaction zone where two adjacent jets met and collided with each other. The in-between jet interference reduces the heat transfer in the interacting zone. The heat transfer depression effect becomes stronger when S/d and H/d ratios are small. Wu et al. [19] investigated the heat transfer and combustion characteristics of small practical RJRC nozzle (producing partially premixed flame ($Re = 8855$)) array suitable for various industrial applications. It was found that the performance of RJRC nozzle in array configuration depends strongly upon the interaction between the neighboring jets. For all nozzle spacings, the flame jets were very stable and very little soot deposition

was observed. Malikov et al. [20,21] investigated the heat transfer characteristics in a specially designed rapid heating experimental furnace equipped with multi-jet combustion chamber for natural gas/air flame (with velocity at the nozzle tip varying from 65 to 400 m/s). The exit of the spent combustion products and the aerodynamics of the adjacent jets in multiple flame jets system are expected to impact pollutant emission and heat transfer in the impinging flame jet arrays. Viskanta [22,23], Baukal and Gebhart [24], and Chander and Ray [25], in their review papers, revealed that the information on arrays of flame jets impingement heat transfer is very scant, despite their wide application in domestic and industrial heating systems.

Detailed and accurate data for the design of equipment using multiple flame jets cannot be predicted from those using single jet because of interaction between neighboring jets. At present, knowledge of the effect of flame jet arrays configuration on heat transfer characteristics is inadequate for the achievement of optimal designs. Most experimental work has been carried out on single flame jets. A complete understanding of the flame structure and heat transfer in practical impinging jet arrays is required. The reviewed literature indicated that all studies on arrays of flame jets have used inline arrangement of jets. Other arrangements have not been studied at all. The interaction between neighboring jets and its effect on heat transfer in case of staggered array arrangement is another interesting configuration that can be studied.

In the present work, an experimental study has been carried out to investigate the heat transfer characteristics of three interacting jet flames (forming a subset of a hexagonal array) located at three vertices of an equilateral triangle (Fig. 15). To the authors' knowledge, this is the first detailed study on a staggered array of flame jets. Effects of inter-jet spacing and separation distance between the plate and the exit plane of the burners have been investigated. The fuel–air mixture used was stoichiometric and the Reynolds number for each of the three jets was 800 for all the operating conditions studied in this work.

2. Experimental setup

Fig. 1 shows the schematic of the experimental setup. Flame impingement heat transfer setup mainly consists of two parts: heat generation and heat absorption. Three copper tubes of inner diameter 6.35 mm placed in a triangular arrangement were used as burners. Fig. 2 shows the schematic for the single tube burner. Each tube has been given a free length of 30–40 d after the flow straightening mesh, which was sufficient to give fully developed flow (parabolic exit velocity profile) at the burner exit. A pair of packings (each consisting of 7–8 fine steel meshes) was used as flame arrestors and was placed at the tail of each burner. Fig. 3 shows schematic arrangement of three interacting impinging jets on a flat surface. Fig. 4 shows the constructional details for the flat plate calorimeter. A copper plate of

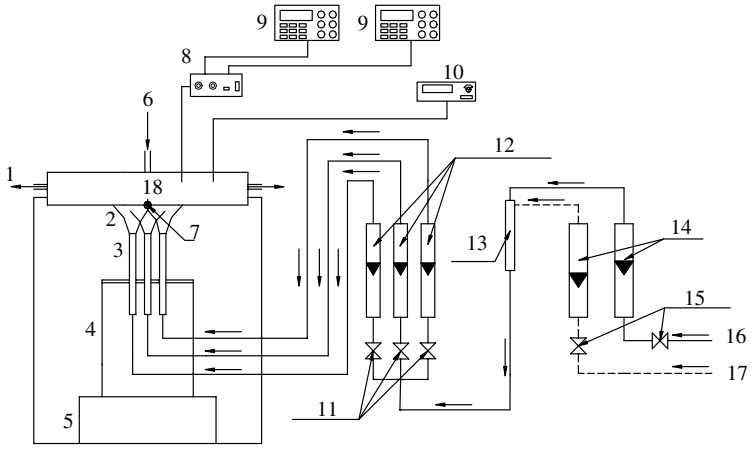

Fig. 1. Schematic of experimental setup for three interacting impinging flame jets: (1) outlet water to waste water tank, (2) interacting flames, (3) burners, (4) burner stand, (5) 3D positioning mechanism, (6) water inlet to calorimeter, (7) heat flux sensor, (8) signal conditioning amplifier, (9) multi-meters, (10) temperature display unit, (11) distributing needle valves, (12) distributing rotameters, (13) mixing tube, (14) air and fuel supply rotameters, (15) needle valves, (16) air from cylinder, (17) methane from cylinder, (18) flat plate calorimeter.

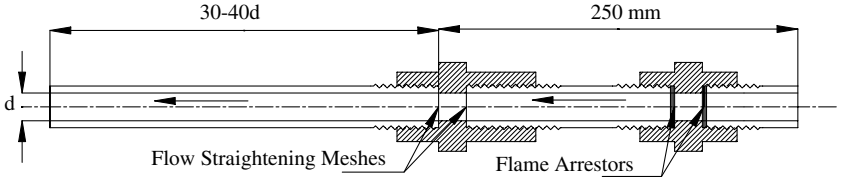

Fig. 2. Burner tube assembly.

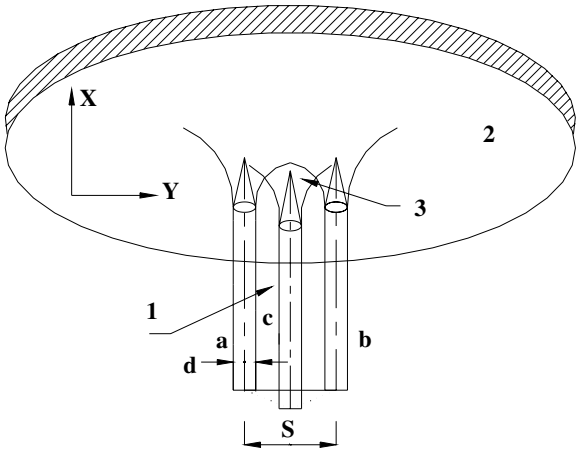

Fig. 3. Schematics of arrangement of three interacting jets impinging on a flat surface: (1) array of burners, (2) impingement surface, (3) interacting flame jets.

8 mm thickness and 300 mm diameter was used as the impingement surface. The surface of the plate was smooth and it did not have any coating on it. There was no soot deposition on the surface; still as precaution it was periodically cleaned. A water jacket was provided at the rear of the copper plate to evenly cool the plate from the backside. A perspex sheet of 10 mm thickness was used as a transparent cover to the cooling jacket to visualize the flow of the cooling water. Water flows into the calorimeter at the center and comes out from the calorimeter through the two exits provided at diametrically opposite points. Inlet and outlet temperatures of the water were measured with T-type thermocouples with full-scale accuracy of ±0.5%. A row of equally spaced K-type thermocouples, in one radial direction, was used to measure the surface temperature. The thermocouples were placed at intervals of 10 mm from each other. The thermocouples were inserted from the rear of the impingement plate by drilling blind holes up to 1 mm from the impingement side. A nickel based anti-seize lubricant was used at the tip of the thermocouple to have good thermal contact with the surface.

The local heat flux (convective plus radiative) on the impingement surface was measured with a single heat flux micro-sensor (HFM) of 6.35 mm diameter (Vatell corporation, HFM-7E/H). This heat flux sensor also has a surface temperature measuring unit. The heat flux and the temperature sensors of the HFM are thin films deposited on the substrate of aluminum nitride. The total thickness of the thin film is less than 2 μm. As a result, the response of HFM is fast, typically less than 10 μs. The heat flux sensor is a differential thermopile, deposited as a precisely registered composite pattern of three materials. The temperature sensor of HFM is a platinum resistor that surrounds the heat flux sensor. Its resistance changes with the surface temperature of the substrate. The surface temperature of the substrate is used to correct the output signal of the heat flux sensor due to the variation of the conductivity of thermal resistance element with temperature. High temperature black paint (Zynolite 1000F) covers the sensor surface with spectral emissivity at 2 μm of 0.94. HFM-7E/H is secured to specially designed copper fixtures. The outer and the inner fixtures were threaded in to the mounting base of the impingement copper plate at the center of the plate with the heat flux sensor flush with the impingement surface. The millivolt (mV) output from the sensor was sensed by a Vatell corporation Model AMP-6 signal conditioning amplifier and directed to a Hewlett Packard Model 34401A Multi-meter. Based on the calibration of HFM-7E/H sensor the appropriate heat flux was calculated from the output of AMP-6 by the software, *Hfcompv4*, provided by the company. Different commercial rotameters were used for measuring the flow rates of air and fuel. Rotameters were calibrated with DryCal DC-Lite (Bios International Corporation) primary gas flow meter. Commercially available methane with 99.99% purity was used and was burnt with synthetic bottled air (volume %: 21% O_2 and 79% N_2). A 3D positioning mechanism was used for the positioning of the burner.

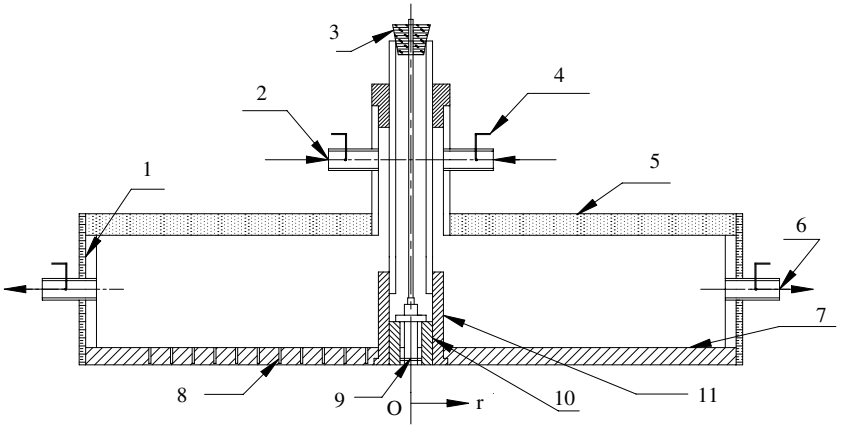

Fig. 4. Flat plate calorimeter: (1) outer jacket insulation, (2) water inlet, (3) cork, (4) T-Type thermocouple, (5) transparent cover, (6) water outlet, (7) copper plate, (8) K-type thermocouples, (9) sensor, (10) inner fixture, (11) outer fixture.

3. Experimental procedure

Measured quantities of air and fuel were mixed in the mixing tube and mixture was fed to the burner. In order to ensure that each burner was operating at identical operating condition, the supply of the fuel/air mixture was measured and controlled by three rotameters connected in the passage of each burner (Fig. 1). Heated water at a temperature range of 35–45 °C was used as the plate coolant to prevent condensation of moisture in the combustion products on the plate. Flow of the cooling water was regulated by calibrated rotameters. Supply of water to the calorimeter was started 15 min before the mixture was ignited. This was to ensure temperature uniformity in the experimental setup. All the readings were taken under steady state when the temperature of the outlet water became constant. Each burner was operated at Reynolds number of 800 under stoichiometric conditions. Effects of inter-jet spacing, S/d, and dimensionless separation distance, H/d were investigated. Four H/d, (2, 2.6 (JT) (tip of the inner reaction cone just touching the target plate), 5 and 7) and four S/d (3, 4, 6 and 7.58) values were selected on the basis of very close, moderate and far away distances. Fig. 5 shows the impingement area under consideration.

Heat flux measurements were recorded along the radial direction for various values θ, starting from $\theta = 0°$. The origin, $r = 0$ was taken to be the centroid of the triangular arrangement, O (Fig. 5). Taking advantage of the symmetry of the system, measurements were taken up to $\theta = 60°$ in angular steps of 10°. In the radial direction all the measurements were taken up to $r = 80$ mm. This radial distance was sufficient to cover the total spread of the flame when the inter-jet spacing was largest. X and Y were the perpendicular axes in the plane of impingement surface with O as the origin. Y-axis was parallel to one of the sides of the triangular arrangement. The size of the plate was very large compared to the spread of the three interacting impinging flame jets. The shaded area (Fig. 5) shows the unit symmetric cell under consideration.

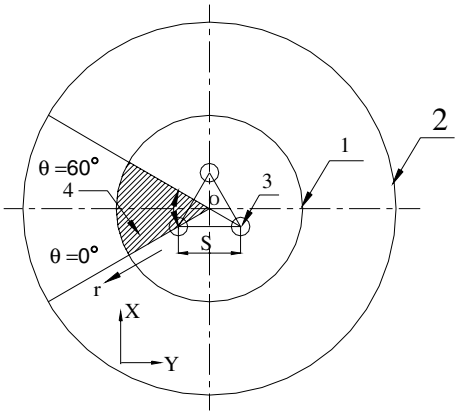

Fig. 5. Heat affected area: (1) measured heat affected area, (2) impingement plate, (3) burner tube, (4) symmetric area under observation.

The flame jet exit Reynolds number was calculated based on cold fuel/air mixture and was given as

$$Re = \frac{u_{\text{exit}} d \rho_{\text{mix}}}{\mu_{\text{mix}}} \quad \text{and} \quad \mu_{\text{mix}} = \frac{\sum(\mu_i y_i \sqrt{M_i})}{\sum(y_i \sqrt{M_i})}$$

The equivalence ratio is defined as

$$\phi = \frac{(A/F)_{\text{stoic}}}{(A/F)_{\text{actual}}}$$

4. Uncertainty analysis

Uncertainty analysis was carried out using the method given by Kline and McClintock [26]. Uncertainties in equivalence ratio and Reynolds number were ±2.83% and ±2.2% respectively. Maximum uncertainty in heat flux measurements was ±5.88%. Full-scale accuracy for T-type thermocouples was ±0.5%. To check the repeatability of the results, five test runs of experiments were conducted under identical operating conditions. Averaging over the repeated runs yielded minimum and maximum deviations in local heat flux of 0.71% and 13.3% of the mean value. Minimum and maximum deviations in average heat flux for the entire plate were found to be 0.88% and 4.25% of the mean value.

5. Results and discussion

5.1. Impinging flame structure

It has been seen that the heat flux distribution on the impingement surface is dependent upon the impinging flame shapes [15,16,27–31]. All the flames were laminar ($Re = 800$) and appeared to be conical in shape with blue inner reaction zone and light blue outer layer. The flame shapes were recorded with a digital camera for different configurations. Burners a and b represent the vertices (Fig. 3) of the triangle on the front side whereas burner c represents the third vertex of the triangle on the other side.

Fig. 6 shows direct photographs of three interacting impinging flame jets with inter-jet spacing, S/d, of 7.58, 4 and 3 and at separation distance, H/d, of 2. At this separation distance, the inner reaction zone was intercepted by the plate. Fig. 6(i) shows the arrangement of flames for $S/d = 7.58$. For this large value of S/d, the flames were located quite far from each other and there was least interaction between the adjacent flames. The between-jets area was devoid of any heating by the flames. For $S/d = 4$ and $H/d = 2$, there was strong interaction between the flames (Fig. 6(ii)). All the flames lifted from the inner periphery and got stabilized like *tilted* flames. The flames were pushed outward from the centroid, possibly because of generation of a pressure around the centroid because of the spent gases. The outer diffusion layers of all the flames merged together. Fig. 6(iii) indicates that the lifting at the burner rim was less for $S/d = 3$ in comparison to $S/d = 4$. Outer

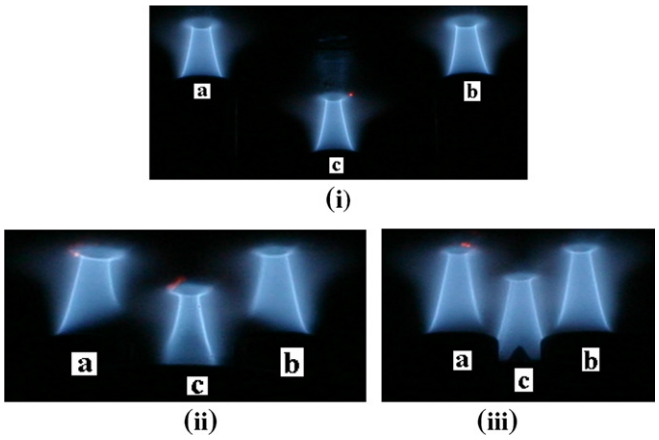

Fig. 6. Direct photographs of three interacting flame jets impinging on the flat surface at $H/d = 2$, $Re = 800$ and $\phi = 1.0$ for $S/d =$ (i) 7.58, (ii) 4 and (iii) 3.

diffusion layers were pushed downward, from the target surface, at the middle of the line joining the stagnation points of two adjacent burners. This was possibly because of pressure generated at the interaction zone [15].

Fig. 7 shows the impinging flame shapes when the tip of the inner reaction zone just touched the impingement surface. In this case, there was no central cool zone since the inner reaction zone was not intercepted by the surface. Again for inter-jet spacing $S/d = 7.58$ (Fig. 7(i)), the three flame jets were almost independent of one another. When the inter-jet spacing was decreased to $S/d = 4$ (Fig. 7(ii)), adjacent jets started interacting with each other. As observed for $H/d = 2$, there was lifting of the flames from the inner side of the burner rim and also the flames were pushed outward because of imbalance of pressure on both the sides of the flame [15]. When the inter-jet spacing was reduced to $S/d = 3$ (Fig. 7(iii)), lift of the flame on the inner side over the burner rim was reduced. Similar to that at $H/d = 2$, there was strong interaction between the flames at $S/d = 3$ and $S/d = 4$.

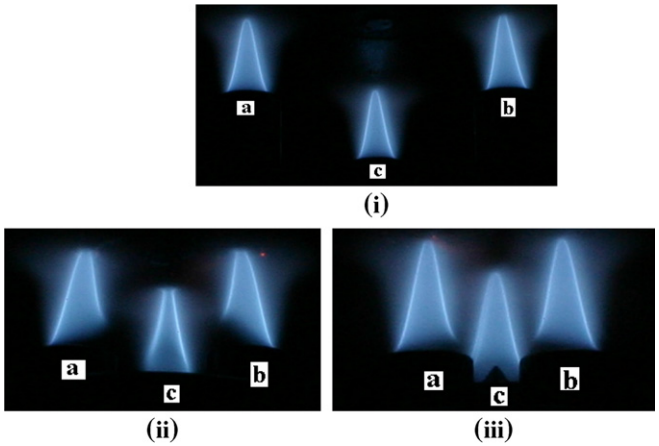

Fig. 7. Direct photographs of three interacting flame jets impinging on the flat surface at $H/d = 2.6$ (JT), $Re = 800$ and $\phi = 1.0$ for $S/d =$ (i) 7.58, (ii) 4 and (iii) 3.

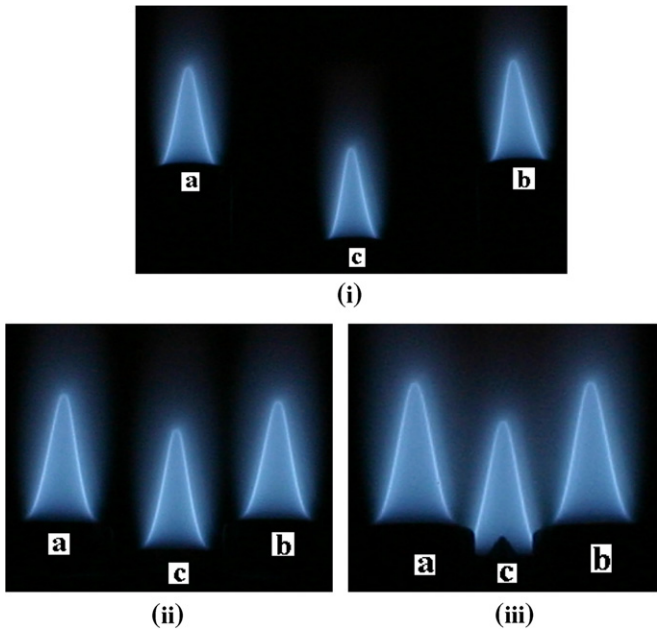

Fig. 8. Direct photographs of three interacting flame jets impinging on the flat surface at $H/d = 5$, $Re = 800$ and $\phi = 1.0$ for $S/d =$ (i) 7.58, (ii) 4 and (iii) 3.

Fig. 8 shows the impinging flame shapes for $H/d = 5$ and inter-jet spacing $S/d = 7.58$, 4 and 3. As shown in Fig. 8(i), at $S/d = 7.58$ flames behaved as independent flame jets. For small inter-jet spacings (Fig. 8(ii) and (iii)), there was some interaction between the outer diffusion layers of the flames. It is interesting to note here that in this case of large separation distance ($H/d = 5$), the flames did not show any tendency to lift off from the inner side of the burners. For this separation distance, the combustion product gases, after impingement on the plate, did not seem to be able to affect the stabilization of the flames on the burners.

5.2. Local heat flux distribution for different configurations

Figs. 9a–9c show the heat flux contours for $H/d = 2$ for various values of S/d. At this separation distance the inner reaction zone was intercepted by the plate. There was impingement of cool fuel/air mixture directly on the surface around the stagnation points of individual jets. This resulted in very low heat flux at all three stagnation points of the impinging flames [15,16,27–31]. Fig. 9a shows the contours of heat flux at $S/d = 3$. An *oval* shape of heat flux contours can be seen because of strong interaction between the adjacent flame jets. The contours were highly compressed on the interacting side and were rarefied on the non-interacting side. Dong et al. [15] also found compressed heat flux contours on the interacting side and mentioned that this was because of pressure difference. Maximum heat fluxes were obtained at those points where the inner reaction zones (of individual jets) were very close to the surface. The area surrounding the centroid had low

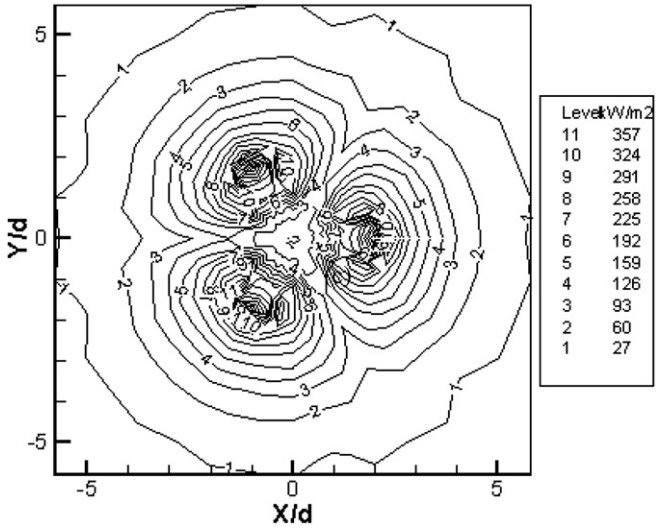

Fig. 9a. Heat flux contours for three methane/air flames impinging on a flat surface with $Re = 800$, $\phi = 1.0$ for $H/d = 2$ and $S/d = 3$.

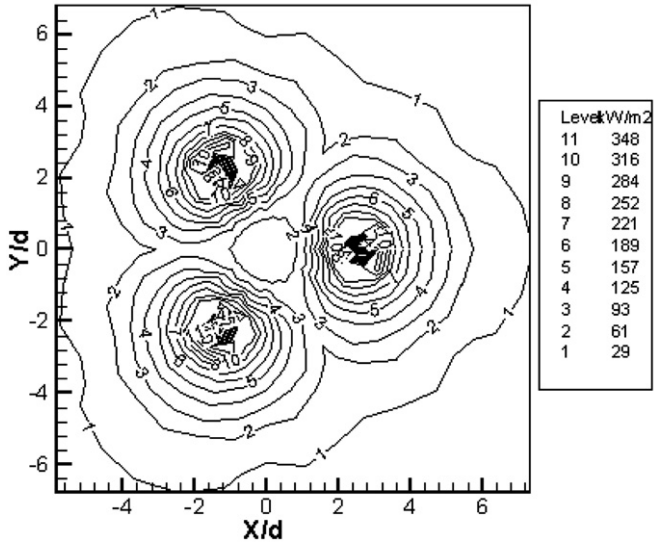

Fig. 9b. Heat flux contours for three methane/air flames impinging on a flat surface with $Re = 800$, $\phi = 1.0$ for $H/d = 2$ and $S/d = 4$.

heat transfer due to the separation of fluid, from the impingement surface, in the vicinity of that zone. This can also be attributed to some positive pressure created due to interaction between the three jets at that point. Goldstein and Timmers [9] also reported a minimum in heat transfer coefficient at the centroid of every triangle formed by 3 neighboring air jets for a system of seven-jet array. Dong et al. [15,16] mentioned that the in-between jet interference reduced the heat transfer in the interacting zone of an in-line array. The heat transfer depression effect became stronger when S/d and H/d ratios were small [15,16].

Heat flux contours were less compressed when S/d was increased to a value of 4 (Fig. 9b). A broader low heat flux zone was formed around the centroid because of larger

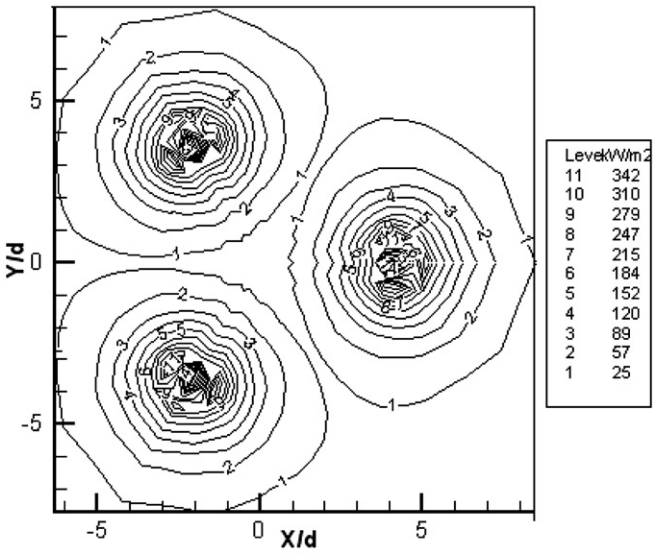

Fig. 9c. Heat flux contours for three methane/air flames impinging on a flat surface with $Re = 800$, $\phi = 1.0$ for $H/d = 2$ and $S/d = 7.58$.

inter-jet distance. Total spread area of the heat flux was more compared to $S/d = 3$ case. Fig. 9c shows the heat flux distribution for very large inter-jet spacing (S/d of 7.58). The compression of heat flux contours on the interacting side was minimal in this case. Peak heat flux values at all inter-jet spacings ($S/d = 3$, 4 and 7.58) were almost same. Direct impingement of cool, unburned mixture led to a lot of variation in heat flux. Therefore at $H/d = 2$, heating was highly non-uniform.

Figs. 10a–10c show the heat flux contours at $H/d = 2.6$ for various values of S/d. At this separation distance the inner reaction zone was just touching the target surface. Peak heat fluxes occurred near stagnation points of the individual impinging jets. These high heat fluxes can be

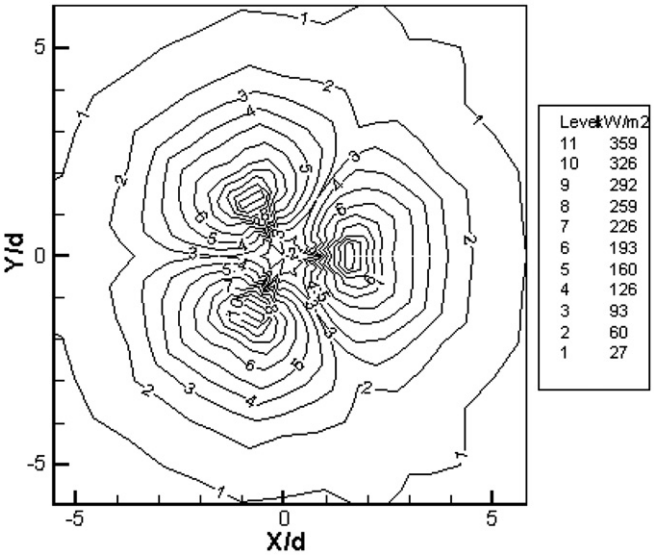

Fig. 10a. Heat flux contours for three methane/air flames impinging on a flat surface with $Re = 800$, $\phi = 1.0$ for $H/d = 2.6$ and $S/d = 3$.

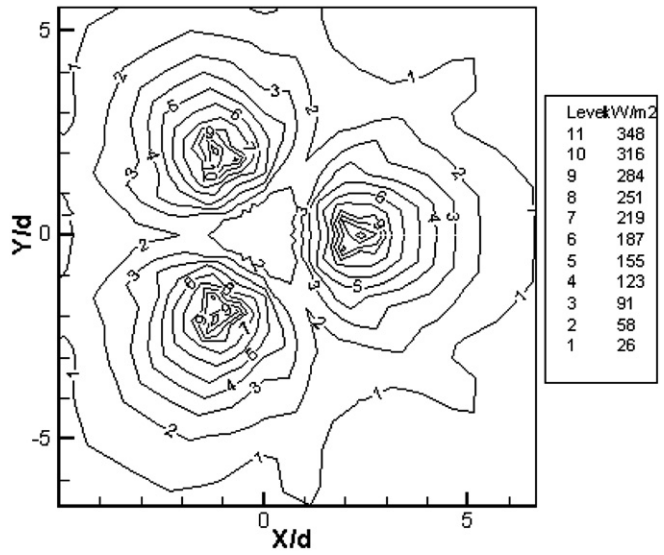

Fig. 10b. Heat flux contours for three methane/air flames impinging on a flat surface with $Re = 800$, $\phi = 1.0$ for $H/d = 2.6$ and $S/d = 4$.

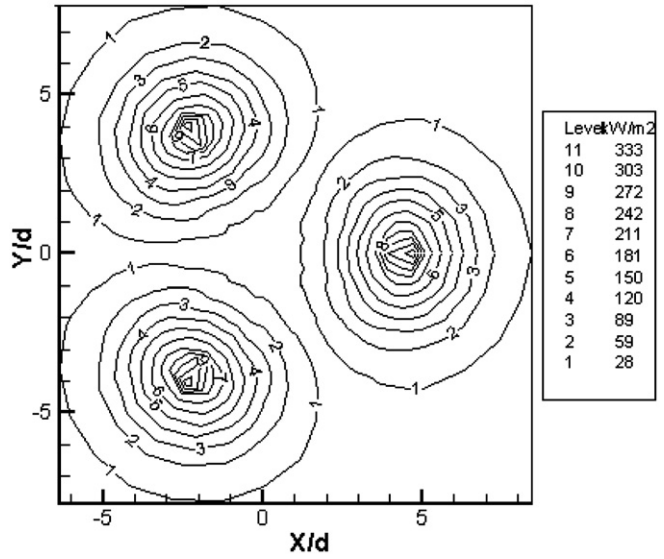

Fig. 10c. Heat flux contours for three methane/air flames impinging on a flat surface with $Re = 800$, $\phi = 1.0$ for $H/d = 2.6$ and $S/d = 7.58$.

attributed to high velocity and temperature of the flame in the vicinity of flame tip. The non-equilibrium nature of the flow in this region also contributes to high heat flux values. Close to the high temperature reaction zone, large concentration of active species such as atoms and free radicals exist which augment convective heat transfer rates by diffusion and exothermic recombination in the boundary layer surrounding the heat receiving body [31,32].

Fig. 10a shows that for small inter-jet spacing ($S/d = 3$), there was strong interaction amongst the impinging flame jets. This resulted in nearly *rectangular* shape of heat flux contours. The contours were highly compressed on the interacting side and rarefied on the non-interacting side. For $S/d = 4$, heat flux contours on the interacting side were more rarefied compared to $S/d = 3$ case (Fig. 10b). Peak heat fluxes observed for $S/d = 3$ and 4 were comparable and the difference was well within the uncertainty range. The central low heat flux zone was larger, as expected. Total spread area of heat transfer was more for $S/d = 4$ compared to $S/d = 3$. A nearly *circular* shape of the heat flux contours can be seen. Fig. 10c shows the heat flux distribution for very large inter-jet spacing (S/d of 7.58) and $H/d = 2.6$ (JT). Heat flux contours were almost equally rarefied on both interacting and non-interacting sides. The shapes of the contours were almost *circular*.

Figs. 11a–11c show the heat flux contours at $H/d = 5$ for various values of S/d. At this separation distance the inner reaction zone was away from the target surface. The peak heat fluxes were substantially less (compared to $H/d = 2$

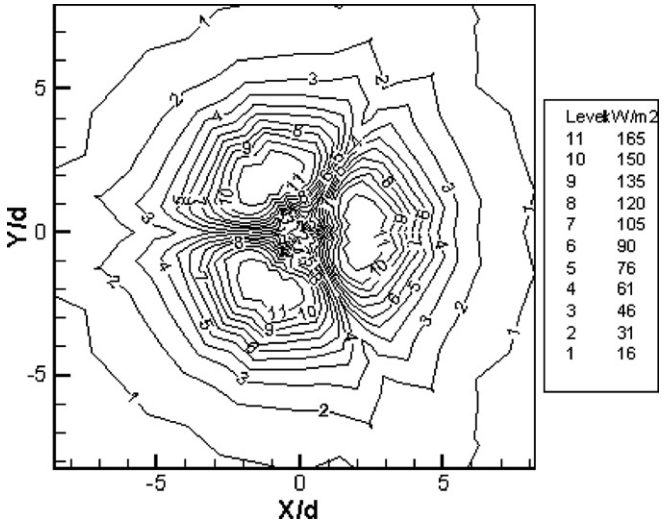

Fig. 11a. Heat flux contours for three methane/air flames impinging on a flat surface with $Re = 800$, $\phi = 1.0$ for $H/d = 5$ and $S/d = 3$.

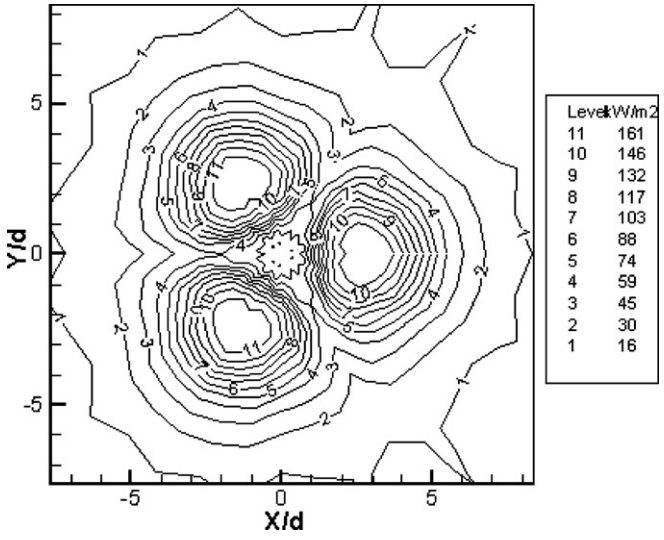

Fig. 11b. Heat flux contours for three methane/air flames impinging on a flat surface with $Re = 800$, $\phi = 1.0$ for $H/d = 5$ and $S/d = 4$.

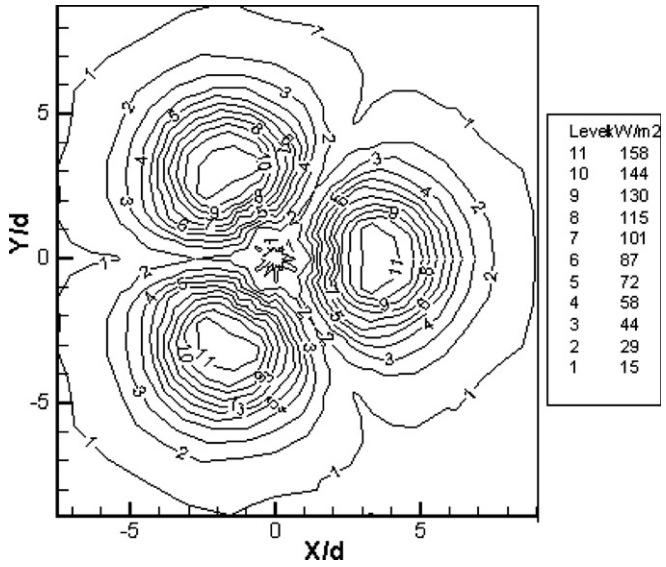

Fig. 11c. Heat flux contours for three methane/air flames impinging on a flat surface with $Re = 800$, $\phi = 1.0$ for $H/d = 5$ and $S/d = 7.58$.

and $H/d = 2.6$ cases) because of the large distance between flame inner reaction zone and the plate. Entrainment of the surrounding air also possibly lowered the temperature of the impinging gas and hence the heat flux. There was a uniformly distributed high heat flux area at the stagnation region of each individual jet.

Fig. 11a shows that for small inter-jet spacing ($S/d = 3$), heat flux contours resembled the shape of a *boat*. Heat fluxes at the centroid were higher compared to those for smaller separation distances. There was a large spread of the jet that helped in more uniform heating compared to smaller H/d cases.

Fig. 11b shows the heat flux contours when the inter-jet spacing was increased to $S/d = 4$. The shape of heat flux contours was not perfectly circular but they were compressed on the interacting side of the jets. The maximum heat flux was distributed over a large area as compared to same configuration ($S/d = 4$) at $H/d = 2$ and 2.6. As discussed in the earlier cases (Figs. 9c and 10c), there was negligible interaction between the adjacent flames at S/d of 7.58 (Fig. 11c). For $H/d = 5$, the heat flux was more uniform over the surface compared to that at smaller H/d values.

5.3. Effect of S/d on heat transfer characteristics

Fig. 12a–c shows the variation in heat flux along $\theta = 0°$ at various inter-jet spacings for fixed separation distance between the exit plane of the burners and the target surface. Fig. 12a shows the heat flux variation along $\theta = 0°$ direction for $H/d = 2$. As discussed earlier, there was a zone of low heat flux around the stagnation point for each of the burners for all S/d. There were two peaks in the heat flux values along this radial direction. For small and intermediate inter-jet spacing ($S/d = 3$, 4 and 6) the inner peak

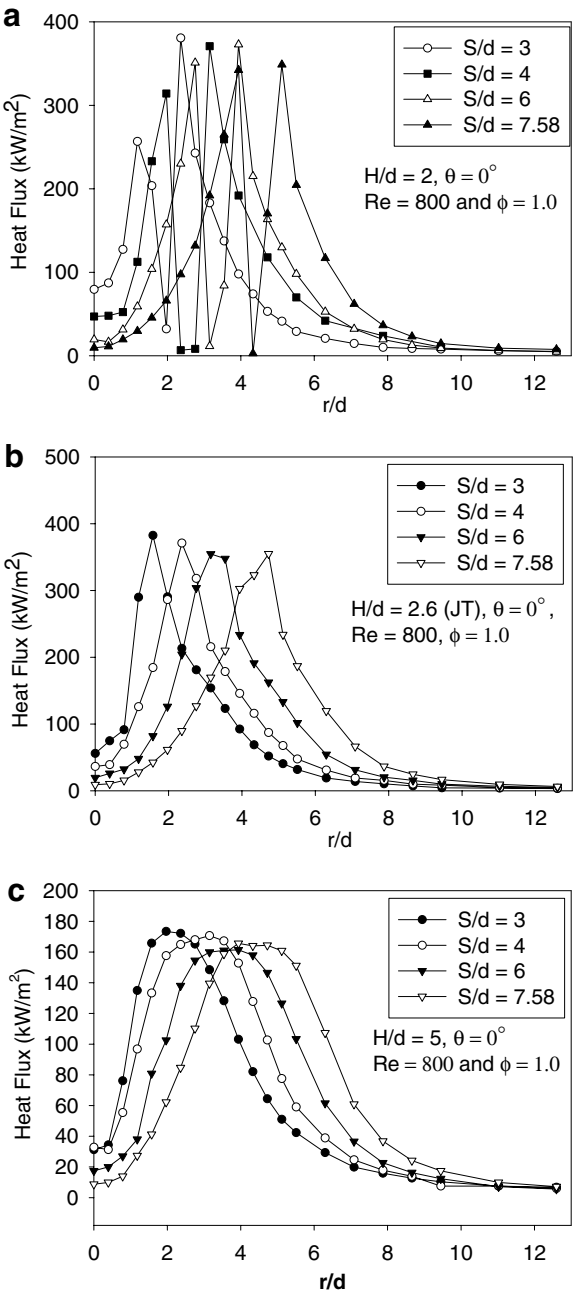

Fig. 12. Heat flux variation along radial direction at $\theta = 0°$ for various S/d, $Re = 800$ and $\phi = 1.0$ and at (a) $H/d = 2$, (b) $H/d = 2.6$ and (c) $H/d = 5$.

value was smaller than the outer peak value. This was possibly because of the outward tilt of the flames due to excess pressure generated by the spent fluid around the centroid. The two peaks for $S/d = 7.58$ (large inter-jet spacing) were comparable because of minimal interaction amongst the jets in this configuration. Peak heat fluxes of 370 kW/m^2, 380 kW/m^2, 372 kW/m^2 and 348 kW/m^2 were obtained for $H/d = 2$ corresponding to non-dimensional inter-jet spacing, S/d, of 3, 4, 6 and 7.58 respectively. Heat flux at the centroid was the highest for $S/d = 3$ and decreased with increase in the value of S/d. Heat flux distribution was highly non-uniform because of the presence of a region

of low heat flux around the stagnation point for each of the burners.

Fig. 12b shows the variation in heat flux along $\theta = 0°$ for $H/d = 2.6$ for various S/d values. At this separation distance the tip of the flame inner reaction zone was just touching the plate. Sharp peaks in the heat flux were observed where the inner reaction zone was close to the surface. This is because of the same reasons as discussed in connection with Fig. 10. Maximum heat fluxes of 382 kW/m^2, 370 kW/m^2, 354 kW/m^2 and 354 kW/m^2 were obtained corresponding to radial locations, r/d, of 1.6, 2.4, 3.2 and 4.7 for values of $S/d = 3$, 4, 6, and 7.58 respectively. Due to very large variation in the heat flux between that at the centroid and the peak heat flux, the heating was quite non-uniform.

Fig. 12c shows the heat flux variation along $\theta = 0°$ for $H/d = 5$ at various inter-jet spacings. There was no sharp peak in the heat flux distributions. Maximum heat fluxes of 173 kW/m^2, 170 kW/m^2, 161 kW/m^2 and 166 kW/m^2 were obtained at radial locations, r/d, of 2, 3.2, 3.9 and 4.7 for values of $S/d = 3$, 4, 6, and 7.58 respectively. These values are substantially lower than the peak heat fluxes for $H/d = 2$ and $H/d = 2.6$. Heat flux at the centroid was lower compared to corresponding values for $H/d = 2$ and 2.6. This is because of less spread of the wall-jet flow in that region. The difference between the peak heat fluxes and the heat fluxes at the centroid was less compared to those at small separation distances ($H/d = 2$ and 2.6). Also, the peak heat fluxes were spread over a large area, resulting in more uniform surface heat flux distribution.

Fig. 13a shows the variation in heat flux along $\theta = 30°$ for different values of S/d and for $H/d = 5$. Along this direction, peak heat flux values were lower than the corresponding values for $H/d = 2$ and 2.6. Peak heat fluxes of 167 kW/m^2, 145 kW/m^2, 122 kW/m^2 and 95 kW/m^2 were obtained at radial locations, r/d, of 2.4, 2.8, 3.2 and 3.9 for values of $S/d = 3$, 4, 6, and 7.58 respectively. Highest peak heat flux was obtained for S/d of 3. This is due to the fact that for this inter-jet spacing, the radial line corresponding to $\theta = 30°$ direction is closest to the stagnation region. Beyond r/d of 4 there was changeover of heat flux trends and the largest inter-jet distance produced the highest heat flux till all the heat fluxes become approximately the same at $r/d = 11$, far away from the centroid. The cross-over takes place because beyond a certain value of r, the distance of the radial location from the nearest burner is minimum when S/d is largest.

Fig. 13b shows the heat flux variation along $\theta = 60°$ for $H/d = 5$ for various values of S/d. The radial line corresponding to $\theta = 60°$ bisects the region between the two adjacent jets (Fig. 5). Thus, along this radial direction, the two streams of wall-jet regions of the adjacent jets interfered with each other. This resulted in a slightly irregular shape of the heat flux distribution. The heat flux values were the largest for the smallest inter-jet spacing. Peak heat fluxes of 65 kW/m^2, 58 kW/m^2, 30 kW/m^2 and 19 kW/m^2 were obtained at radial locations, r/d, of 2, 2, 2.7 and 3.5 for values of $S/d = 3$, 4, 6, and 7.58 respectively. The heat flux at the centroid was the highest for $S/d = 4$. For large inter-jet spacing, heat flux values were quite low along this direction.

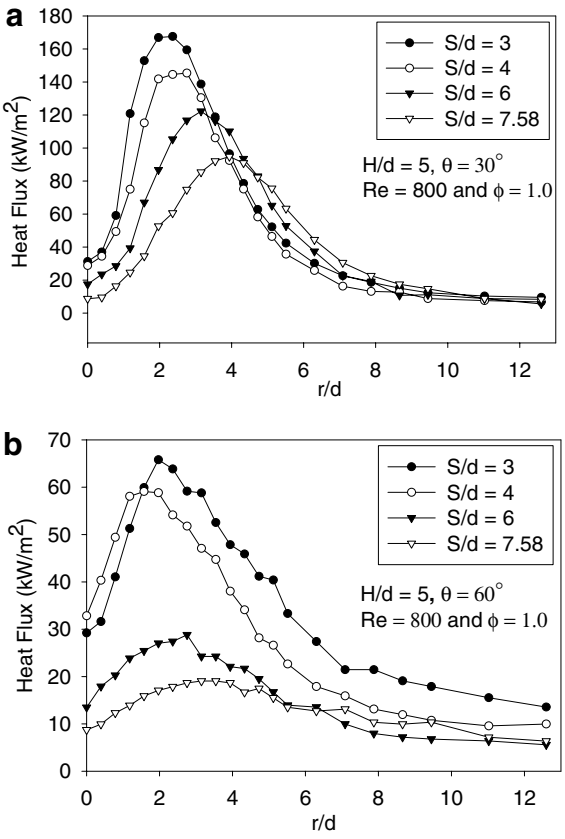

Fig. 13. Heat flux variation along radial direction for various S/d and at $H/d = 5$, $Re = 800$ and $\phi = 1.0$ and at (a) $\theta = 30°$ and (b) $\theta = 60°$.

5.4. Effect of H/d on heat transfer characteristics

Fig. 14a–c shows the variation in heat flux along $\theta = 0°$, 30° and 60° for various values of H/d and for $S/d = 3$. Fig. 14a shows the heat flux distributions along $\theta = 0°$. For $H/d = 2$, there is a dip in the heat flux profile because of impingement of cool un-burnt mixture on the plate. There are two peaks in the heat flux profile for this separation distance. The magnitude of the inner peak was less compared to the outer peak because of the outward tilt of the flame due to pressure generated by the spent gases at and around the centroid. The peak heat fluxes were obtained at or near the stagnation points (except when the inner reaction zone was intercepted by the surface). This is because of two reasons: first, the inner reaction zone at those points is very close to the surface which ultimately gives higher temperature gradient and second, the convection heat transfer effect is very strong near the stagnation point, in the early wall-jet region.

The peak heat fluxes of 380 kW/m^2, 382 kW/m^2, 173 kW/m^2 and 157 kW/m^2 were obtained for $S/d = 3$ for non-dimensional impingement heights (H/d) of 2, 2.6, 5

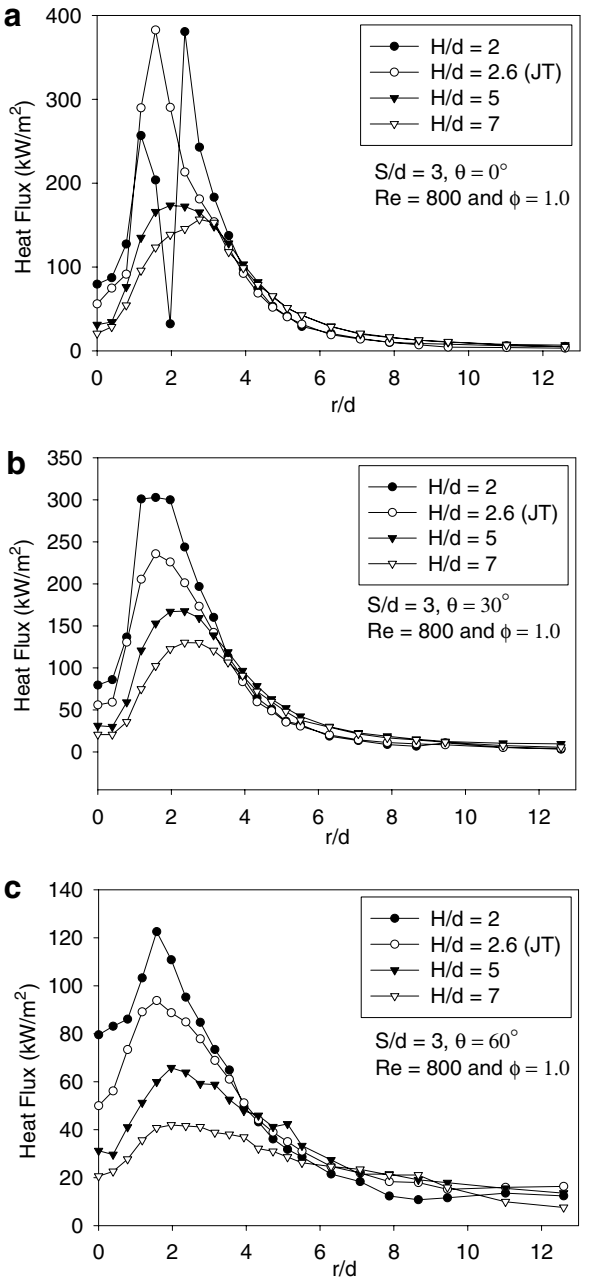

Fig. 14. Heat flux distribution for $S/d = 3$ at various H/d at $Re = 800$ and $\phi = 1.0$ and (a) $\theta = 0°$, (b) $\theta = 30°$ and (c) $\theta = 60°$.

and 7 respectively. Heat fluxes at the centroid are higher for smaller separation distances because of greater spread of the flame over the surface. Maximum heat flux was attained at the stagnation point when the tip of the inner reaction zone just touched the target surface, i.e., at $H/d = 2.6$. At higher non-dimensional separation distances, i.e., at $H/d = 5$ and 7, the maximum heat flux was less because of larger distance between the inner reaction zone and the target surface. For $r/d > 4$ the heat flux trends were similar for all separation distances. This is because, in case of jet impingement heating, most of the heat transfer is in the stagnation and early wall-jet regions.

Fig. 14b presents the heat flux distributions at various separation distances and for inter-jet spacing of $S/d = 3$ along $\theta = 30°$. The heat flux at the centroid was higher for smaller separation distances because of greater spread of the flame in that region. The maximum heat flux along this direction occurred at $H/d = 2$, since in this case, there was a greater spread of the flame on the target plate and the $\theta = 30°$ direction was closer to the flame compared to cases with higher H/d values. The maximum heat fluxes of 300 kW/m^2, 235 kW/m^2, 168 kW/m^2 and 130 kW/m^2 occurred at non-dimensional radial locations, r/d, of 2, 1.6, 2.4 and 2.4 for non-dimensional heights, H/d, of 2, 2.6, 5, and 7 respectively. The heat flux variation along this direction is quite appreciable for stagnation and early wall-jet regions of the impinging jet. There was not much difference in the heat flux distributions beyond $r/d \geqslant 3.9$.

Fig. 14c shows the radial heat flux distributions along $\theta = 60°$ for various separation distances and for S/d of 3. Heat flux was maximum at the centroid for minimum separation distance of $H/d = 2$. The heat flux values at the centroid were 79 kW/m^2, 50 kW/m^2, 31 kW/m^2 and 20 kW/m^2 for dimensionless separation distances of $H/d = 2$, 2.6, 5 and 7 respectively. With increase in separation distance the peak heat flux decreased. Maximum heat fluxes of 122 kW/m^2, 94 kW/m^2, 65 kW/m^2 and 41 kW/m^2 occurred at radial locations, r/d, of 1.6, 1.6, 2 and 2 for non-dimensional heights, H/d, of 2, 2.6, 5, and 7 respectively.

5.5. Comparison of heat flux distributions on the basis of average heat flux and rms deviation of average heat flux

From the viewpoint of practical applications, it is important to express the results in the form of average heat flux to the surface. The surface average heat flux was obtained by area-weighted method as given in Eq. (1). For each burner, a hexagonal area around the burner (as shown in Fig. 15) is considered to be the zone affected by that burner [33]. Thus, for a given system of three interacting jets, an area-weighted average was carried out over the entire area of three hexagons as shown in Fig. 15.

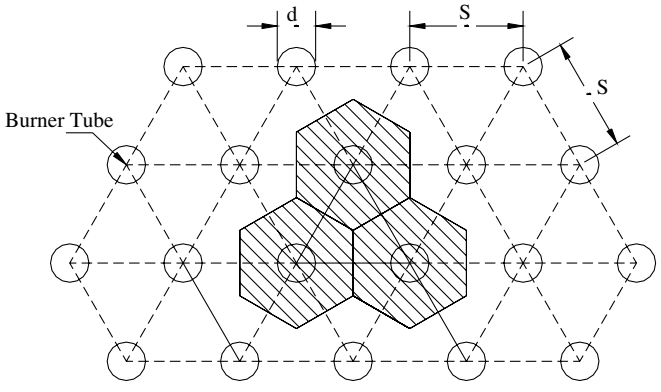

Fig. 15. Integration areas (shaded) for average heat transfer calculation.

To compare the uniformity in heating at different values of S/d and H/d, rms deviation and percentage relative deviation of heat flux from average heat flux value were obtained using Eqs. (2)–(4):

$$\dot{q}''_{\text{avg}} = \frac{1}{A}\int \dot{q}''\,\mathrm{d}A \tag{1}$$

$$\dot{q}''_{\text{dev}} = \dot{q}''_{\text{avg}} - \dot{q}'' \tag{2}$$

$$\dot{q}''_{\text{dev,rms}} = \sqrt{\frac{\sum(\dot{q}''_{\text{dev}})^2}{n}} \tag{3}$$

$$\text{relative deviation} = \frac{\dot{q}''_{\text{dev,rms}}}{\dot{q}''_{\text{avg}}} \times 100\% \tag{4}$$

Table 1 indicates that when the separation distance was small, i.e., at $H/d = 2$ and $H/d = 2.6$, the heat fluxes observed were very high. Hou and Ko [34] had also observed that the maximum heating efficiency was obtained when the inner reaction zone was intercepted by the plate (type-C flame in their study). It was also mentioned that interception of the flame makes the high temperature zone in the flame wider, resulting in high heat transfer rate. In the present work high average heat fluxes were obtained at small H/d and S/d values. As the separation distance was increased to $H/d = 5$, the average heat fluxes decreased because the inner reaction zone was far away from the target surface. Large gap between the tip of the inner reaction zone and the plate caused a reduction in the thermal performance of the flame jet system due to entrainment of surrounding air. When separation distance was further increased to $H/d = 7$, the average heat flux decreased to a minimum value because of excessive entrainment of outside air. The average heat flux also decreased with increase in inter-jet spacing, S/d. The low heat flux area around centroid increases with increase in S/d, resulting in decrease in average heat flux. It can thus be concluded that to have high average heat fluxes for the set of three interacting flames under consideration, both inter-jet spacing and separation distance should be small.

Other parameter that is of great importance in flame impingement heating is the uniformity in surface heat flux. To compare the heat flux uniformity for different configurations percentage relative deviation of heat flux values from average heat flux was calculated for each configuration (Table 2). Relative deviation in average heat flux increased with S/d. So for small inter-jet spacing the heating was more uniform compared to large inter-jet spacing. Also, the relative deviation decreased with increase in separation distance from $H/d = 2$ to $H/d = 5$. With further increase in H/d to the value of 7, the relative deviation increased. Also at very large separation distances average heat flux was very less. Thus, large separation distances are not acceptable from the viewpoint of effective heating. At $H/d = 5$, the average heat flux was reasonably good and at the relative deviation was also less. Thus, for the configurations studied, $H/d = 5$ can be considered as an optimum separation distance at which we can get optimum average heat flux and uniformity in the heating. Dong et al. [15] has also observed that for three inline interacting jet system the optimum heat transfer was at $H/d = 5$. The configuration $H/d = 5$, $S/d = 3$ gives minimum relative deviation in average heat flux. So it can be concluded that for three interacting flame jet system (forming a subset of a hexagonal staggered array) studied here, $H/d = 5$ and $S/d = 3$ is the optimum configuration.

Table 1
Average heat flux (kW/m^2) corresponding to different values of inter-jet spacing and at different separation distances

	$H/d = 2$	$H/d = 2.6$ (JT)	$H/d = 5$	$H/d = 7$
$S/d = 3$	194.6	175.3	134.6	105.9
$S/d = 4$	192.5	142.7	119.7	99.1
$S/d = 6$	91.0	93.0	84.9	72.9
$S/d = 7.58$	78.6	79.2	67.9	49.6

Table 2
Relative deviation (%) in heat flux from average value for different values of inter-jet spacing and at different separation distances

	$H/d = 2$	$H/d = 2.6$ (JT)	$H/d = 5$	$H/d = 7$
$S/d = 3$	42.08	40.15	30.98	37.01
$S/d = 4$	46.85	51.50	33.24	39.25
$S/d = 6$	82.74	77.63	53.00	51.57
$S/d = 7.58$	95.54	87.75	67.89	74.19

5.6. Comparison with single jet

For comparing the heat flux characteristics of single isolated flame jet and the triangular array under consideration, experiments were performed under similar conditions. Heat flux variation as a function of r/d for a single isolated flame jet was compared against that for an array with $S/d = 4$ along $\theta = 0°$ direction. It was found that the interference between the adjacent jets had a significant effect on the heat transfer characteristics of the interacting jets.

Fig. 16 shows the comparison of results for single isolated jet and array of interacting jets. Comparison is

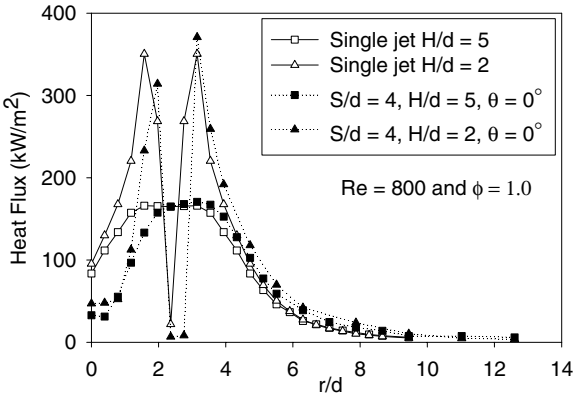

Fig. 16. Comparison of heat flux variation along $\theta = 0°$ for $S/d = 4$ with single jet at $H/d = 2$ and 5 for $Re = 800$ and $\phi = 1.0$.

presented for $H/d = 2$ and 5. There was no significant difference in peak heat flux values (for both H/d values) for single isolated jet and interacting jet. Due to interaction between the adjacent jets there was a shift in the heat flux curves in the outward direction for interacting jets. This was because of pushing of the flames due to pressure generated at the centroid by the spent gases. For interacting flame jets at $H/d = 2$, unlike single isolated jet, the two peaks of heat flux were of different magnitudes. The strong interaction between the jets leads to outward tilt of the flames resulting in lower heat flux on the inner side. Heat flux at the centroid was higher for isolated single jet compared to interacting jet.

6. Conclusions

An experimental study has been carried out for three interacting methane/air flame jets impinging on a flat surface and the following conclusions were arrived at:

1. The heat transfer characteristics were intimately related to flame shapes. Very high heat fluxes were obtained when the conical inner reaction zone was in close proximity of the surface.
2. There was strong interaction between the adjacent jets when the inter-jet spacing and the separation distance were small. Interaction resulted in the flames lifting off the burner rim on the inner, interacting side. The flames were attached to the outer side of the burner rim and stabilized in the form of tilted flames.
3. At small inter-jet spacings, the heat flux contours were compressed on the interacting side and rarefied on the non-interacting side. At the centroid of the triangle a minimum in heat flux was observed.
4. Average heat fluxes were high at small separation distances and at small inter-jet spacings but the heat flux distribution was quite non-uniform. Again, at very large separation distances the heat flux distribution was non-uniform. The heating was most uniform at a moderate separation distance of $H/d = 5$.
5. The average heat flux decreased with increase in inter-jet spacing. Also, the heating was non-uniform at large inter-jet spacings because of the presence of low heat flux region between the jets. At very small inter-jet spacing ($S/d = 3$) the heating was most uniform. For the system of three interacting flame jets under consideration, $H/d = 5$ and $S/d = 3$ was found to be the optimum configuration.

Acknowledgements

The first author is thankful to All India Council of Technical Education (AICTE) for sponsoring him for this research program. He is also thankful to National Institute of Technology, Jalandhar (Punjab) for granting him study leave for this research.

References

[1] K.R. Saripalli, Visualization of multi-jet impingement flow, AIAA J. 21 (4) (1983) 483–484.
[2] Jung-Yang San, Mao-De Lai, Optimum jet-to-jet spacing of heat transfer for staggered arrays of impinging air jets, Int. J. Heat Mass Transfer 44 (2001) 3997–4007.
[3] A.I. Behbahani, R.J. Goldstein, Local heat transfer to staggered arrays of impinging circular air jets, ASME J. Eng. Power 105 (1983) 354–360.
[4] R.J. Goldstein, W.S. Seol, Heat transfer to a row of impinging circular air jets including the effect of entrainment, Int. J. Heat Mass Transfer 34 (8) (1991) 2133–2147.
[5] D.E. Metzger, L.W. Florschuetz, D.I. Takeuchi, R.D. Behee, R.A. Berry, Heat transfer characteristics for inline and staggered arrays of circular jets with cross-flow of spent air, ASME J. Heat Transfer 101 (1979) 526–531.
[6] M. Can, A.B. Etemoglu, A. Avci, Experimental study of convective heat transfer under arrays of impinging air jets from slot and circular holes, Heat Mass Transfer 38 (2002) 251–259.
[7] A.M. Huber, R. Viskanta, Effect of jet-jet spacing on convective heat transfer to confined impinging arrays of axisymmetric air jets, Int. J. Heat Mass Transfer 37 (18) (1994) 2859–2869.
[8] A.M. Huber, R. Viskanta, Comparison of convective heat transfer to perimeter and center jet in a confined, impinging array of axisymmetric air jets, Int. J. Heat Mass Transfer 37 (18) (1994) 3025–3030.
[9] R.J. Goldstein, J.F. Timmers, Visualization of heat transfer from arrays of impinging jets, Int. J. Heat Mass Transfer 25 (12) (1982) 1857–1868.
[10] L.F.G. Geers, J.F. Timmers, K. Hanjalic, Experimental investigation of impinging jet arrays, Exp. Fluids 36 (2004) 946–958.
[11] N.T. Obot, T.A. Trabold, Impingement heat transfer within arrays of circular jets: Part 1 – effect of minimum, intermediate, and complete cross-flow for small and large spacings, ASME J. Heat Transfer 109 (1987) 872–879.
[12] N.R. Saad, S. Polat, W.J.M. Douglas, Confined multiple impinging slot jets without cross-flow effects, Int. J. Heat Fluid Flow 13 (1) (1992) 2–14.
[13] S.J. Slayzak, R. Viskanta, F.P. Incropera, Effect of interaction between the adjoining rows of circular free-surface jets on local heat transfer from the impinging surface, ASME J. Heat Transfer 116 (1994) 88–95.
[14] L.W. Florschuets, C.C. Su, Effect of cross-flow temperature on heat transfer within an array of impinging jets, ASME J. Heat Transfer 109 (1987) 74–82.
[15] L.L. Dong, C.S. Cheung, C.W. Leung, Heat transfer of row of three butane/air flame jets impinging on a flat plate, Int. J. Heat Mass Transfer 46 (2003) 113–125.
[16] L.L. Dong, C.S. Cheung, C.W. Leung, Heat transfer and wall pressure characteristics of twin premixed butane/air flame jets, Int. J. Heat Mass Transfer 47 (2004) 489–500.
[17] L.L. Dong, C.S. Cheung, C.W. Leung, Structure and heat transfer of premixed butane/air flame jets impinging on the flat surface, in: Proceedings of 2001 Technical Meeting, Eastern State Section of The Combustion Institute, December 2–5, 2001, Hilton Head, South California, 2001, pp. 392–395.
[18] L.L. Dong, C.S. Cheung, C.W. Leung, Heat transfer characteristics of a pair of impinging rectangular flame jets, J. Heat Transfer 125 (2003) 1040–1046.
[19] J. Wu, J. Sayed Yagoobi, R.H. Page, Heat transfer and combustion characteristics of an array of radial jet re-attachment flames, Combust. Flames 125 (2001) 955–964.
[20] G.K. Malikov, D.L. Lobanov, K.Y. Malikov, V.G. Lisienko, R. Viskanta, A.G. Fedorov, Direct flame impingement heating for rapid thermal material processing, Int. J. Heat Mass Transfer 44 (2001) 1751–1758.

[21] G.K. Malikov, D.L. Lobanov, K.Y. Malikov, V.G. Lisienko, R. Viskanta, A.G. Fedorov, Experimental and numerical study of heat transfer in flame jet impingement system, J. Inst. Energy 72 (1999) 2–9.
[22] R. Viskanta, Heat transfer to impinging isothermal gas and flame jets, Exp. Thermal Fluid Sci. 6 (1993) 111–134.
[23] R. Viskanta, Convective and radiative flame jet impingement heat transfer, Int. J. Transport Phenomenon 1 (1998) 1–15.
[24] C.E. Baukal, B. Gebhart, A review of flame impingement heat transfer. part 1: experimental conditions, Combust. Sci. Technol. 104 (1995) 339–357.
[25] S. Chander, A. Ray, Flame impingement heat transfer – a review, Energy Convers. Manage. 46 (18–19) (2005) 2803–2837.
[26] S.J. Kline, F.A. McClintock, Describing uncertainties in single sample experiments, Mech. Eng. 75 (1953) 3–8.
[27] L.L. Dong, Studies of single and multiple impinging hydrocarbon flame jets, Ph.D. Thesis, Hong Kong Polytechnic University, Hong Kong, 2002.
[28] L.C. Kwok, C.S. Cheung, C.W. Leung, Heat transfer characteristics of slot and round pre-mixed impinging butane/air flame jet, Exp. Heat Transfer 16 (2003) 111–137.
[29] A. Milson, N.A. Chigier, Studies of methane air flames impinging on cold plate, Combust. Flame 21 (1973) 295–305.
[30] J.R. Rigby, B.W. Webb, An experimental investigation of diffusion flame jet impingement heat transfer, in: L.S. Fletcher, T. Aihara (Eds.), Proceedings of the ASME/JSME Thermal Engineering Joint Conference 1995, Vol. 3, ASME, New York, 1995, pp. 117–126.
[31] S. Chander, A. Ray, Influence of burner geometry on heat transfer characteristics of methane/air flame impinging on flat surface, Exp. Heat Transfer 19 (1) (2006) 15–38.
[32] G.K. Hargrave, M. Fairweather, J.K. Kilham, Forced convection heat transfer from impinging flames. Part II: impingement heat transfer, Int. J. Heat Mass Transfer 8 (1987) 132–138.
[33] H. Martin, Heat and mass transfer between impinging gas jets and solid surface, in: T. Irvine, J.P. Harnett (Eds.), Advances in Heat Transfer, vol. 13, Academic Press, New York, 1970, pp. 1–60.
[34] S.S. Hou, Y. Ko, Effects of heating height on flame appearance, temperature field and efficiency of an impinging laminar jet flame used in domestic gas stoves, Energy Convers. Manage. 45 (9–10) (2004) 1583–1595.